

## Evaluating x-ray detectors for radiographic applications: A comparison of ZnSCdS:Ag with Gd<sub>2</sub>O<sub>2</sub>S:Tb and Y<sub>2</sub>O<sub>2</sub>S:Tb screens

I Kandarakis†, D Cavouras†||, G S Panayiotakis‡ and C D Nomicos§

† Department of Medical Instrumentation Technology, Technological Educational Institution of Athens, Ag Spyridonos Street, Aigaleo 122 10, Athens, Greece

‡ Department of Medical Physics, Medical School, University of Patras, 265 00 Patras, Greece

§ Department of Electronics, Technological Educational Institution of Athens, Ag Spyridonos Street, Aigaleo, Athens, Greece

Received 12 September 1996, in final form 17 March 1997

**Abstract.** ZnSCdS:Ag was evaluated as a radiographic image receptor and was compared with Gd<sub>2</sub>O<sub>2</sub>S:Tb and Y<sub>2</sub>O<sub>2</sub>S:Tb phosphors often used in radiography. The evaluation of a radiographic receptor was modelled as a three-step process: (i) determination of light output intensity as related to the input radiation dose, (ii) determination of visible light characteristics with respect to radiographic optical detectors, and (iii) determination of image information transfer efficiency. The light intensity emitted per unit of x-ray exposure rate was measured and theoretically calculated for laboratory prepared screens with coating thicknesses from 20 to 220 mg cm<sup>-2</sup> and tube voltages from 50 to 250 kVp. ZnSCdS:Ag light intensity was higher than that of Gd<sub>2</sub>O<sub>2</sub>S:Tb or Y<sub>2</sub>O<sub>2</sub>S:Tb for tube voltages less than 70 and 80 kVp respectively. ZnSCdS:Ag displayed the highest x-ray to light conversion efficiency (0.207) and had optical properties close to those of Gd<sub>2</sub>O<sub>2</sub>S:Tb and Y<sub>2</sub>O<sub>2</sub>S:Tb, and its emission spectrum was well matched to optical detectors. The image information transfer properties described by the modulation transfer function, the quantum noise transfer function, and the detective quantum efficiency were calculated for both general radiographic and mammographic conditions and were found to be intermediate between those of Gd<sub>2</sub>O<sub>2</sub>S:Tb and Y<sub>2</sub>O<sub>2</sub>S:Tb screens. Conclusively, ZnSCdS:Ag is an efficient phosphor well suited to radiography.

### 1. Introduction

Silver-activated zinc–cadmium sulphide (ZnSCdS:Ag) is a phosphor material of relatively short decay time that has been widely used in electron to light converting screens, as in TV tubes and in image intensifiers (*Lumilux Data Book* 1989). Initial results on the luminescence of ZnSCdS:Ag phosphor screens have been obtained under radioactive isotope excitation (Ludwig 1971) or under fluoroscopic conditions (Nomicos *et al* 1978) in transmission mode of measurement, referring to front screen-photocathode configuration of image intensifiers. Both studies reported high luminescence efficiencies for ZnSCdS:Ag phosphor, better than those of CaWO<sub>4</sub>:Pb, CsI:Tl, or Gd<sub>2</sub>O<sub>3</sub>:Eu (Ludwig 1971). To our knowledge, ZnSCdS:Ag has never been studied under radiographic conditions and it has never been employed in x-ray to light converting intensifying screens used in radiographic cassettes or in digital radiography systems.

§ Please address correspondence to Professor D Cavouras, PhD, Department of Medical Instrumentation Technology, 37–39 Esperidon Street, Kallithea 17671, Athens, Greece. E-mail address: cavouras@hol.gr

In the present study a systematic investigation of the suitability of the ZnSCdS:Ag phosphor to be employed in x-ray general radiography and mammography screens was carried out. ZnSCdS:Ag phosphor was compared with Gd<sub>2</sub>O<sub>2</sub>S:Tb and Y<sub>2</sub>O<sub>2</sub>S:Tb phosphors, often used in the intensifying screens of conventional radiographic cassettes and in the phosphor screens of digital radiography systems (Arnold 1979, Zweig and Zweig 1983, Morgan *et al* 1987, Gurwich 1995, Maidment and Yaffe 1995). Phosphor materials were employed in the form of laboratory-prepared test screens and the following were evaluated: (i) the x-ray luminescence efficiency under radiographic conditions, (ii) the intrinsic x-ray to light conversion efficiency, (iii) the emitted light spectrum and its spectral compatibility to optical photon detectors (films, photodiodes), (iv) the light attenuation coefficients, absorption, scattering, and reflection, and (v) the image information transfer characteristics, MTF (modulation transfer function), QNTF (quantum noise transfer function), and DQE (detective quantum efficiency) for both radiographic and mammographic applications.

## 2. Materials and methods

The performance evaluation of radiographic phosphor screens comprised three main stages. First, the phosphor's efficiency as an x-ray to light converter was studied by determining the intensity of light emission (luminescence) with respect to the incident x-ray beam intensity. The latter is related to the radiation dose delivered to the patient. Second, the phosphor's coupling efficiency to optical photon detectors used in radiography (films, photodiode arrays) was evaluated by measuring the emitted optical spectrum and determining how well this spectrum is captured by optical detectors. Third, the image information transfer efficiency of the phosphor, giving the information content of the produced diagnostic image, was studied by evaluating the MTF, QNTF, and DQE for both general radiographic and mammographic imaging.

### 2.1. X-ray to light conversion efficiency (absolute efficiency)

X-ray luminescence efficiency characterizes the ability of a phosphor x-ray image detector to produce an adequately bright image at reduced patient doses. The x-ray luminescence efficiency may be expressed by the ratio of the light flux emitted towards the observation side divided by the incident x-ray exposure rate; this ratio is also called absolute efficiency (AE). The AE of the ZnSCdS:Ag phosphor material was studied by employing both experimental and theoretical methods.

For AE measurements the following equipment was employed: (i) a Siemens Stabilipan x-ray unit with tube voltages ranging from 50 to 250 kVp, (ii) an EMI 9558 QB photomultiplier with an extended S-20 photocathode coupled to a Cary 401 vibrating reed electrometer, for light flux measurements, and (iii) a PTW Simplex dosimeter, employed for exposure rate measurements. The phosphor material used was ZnS<sub>60</sub>CdS<sub>40</sub>:Ag, which was supplied by Derby Luminescence, UK, in powder form with 10  $\mu\text{m}$  grain size (code ZDB/F3). Phosphor screens were prepared by sedimentation (Nomicos *et al* 1978) of the phosphor powder on silica substrates with screen coating thicknesses 20, 35, 55, 70, 82, 114, 145 and 220  $\text{mg cm}^{-2}$ . Phosphor screens of Gd<sub>2</sub>O<sub>2</sub>S:Tb (code GT1016) and Y<sub>2</sub>O<sub>2</sub>S:Tb (code YTO/70) were similarly prepared for comparison with the ZnSCdS:Ag screens.

The variation of AE with x-ray tube voltage and phosphor coating thickness was experimentally determined in both transmission and reflection modes of measurement (Giakoumakis *et al* 1990, Kandarakis *et al* 1996, Panayiotakis *et al* 1996). In transmission mode light emitted from the screen surface opposite to that of the x-ray beam incidence

was measured, while in reflection mode light emitted by the surface receiving the x-rays was recorded. The first mode concerns the front screen–radiographic film configuration in radiographic cassettes and the phosphor screen–CCD array combination in digital radiography. The second mode corresponds to rear-intensifying screens used in double-coated radiographic cassettes or in single-coated mammographic cassettes.

Absolute efficiency was theoretically evaluated (see appendix A) considering the product of three quantities (Ludwig 1971):

$$AE(E, T) = A_Q(E, T)n_c G_L(\sigma, \beta, \rho, E, T) \quad (1)$$

where  $A_Q(E, T)$  is the x-ray quantum detection efficiency (QDE), expressing the fraction of incident x-ray quanta detected by the screen, given by

$$A_Q(E, T) = 1 - \exp[-\mu(E)T] \quad (2)$$

where  $\mu(E)$  is the mass attenuation coefficient of ZnSCdS:Ag for x-rays of energy  $E$  in kiloelectron volts, calculated from values for Zn, S and Cd taken from the work of Storm and Israel (1967) and Saloman *et al* (1988), and  $T$  is the screen coating thickness.  $n_c$  is the intrinsic x-ray to light conversion efficiency, giving the fraction of absorbed x-ray energy converted to light within the phosphor material, and  $G_L(\sigma, \beta, \rho, E, T)$  is the light transmission efficiency, expressing the fraction of light produced that reaches the screen output.  $\sigma$ ,  $\beta$  and  $\rho$  are optical parameters related to light absorption, light scattering, and light reflectivity (Ludwig 1971) as follows:

$$\sigma = [a(a + 2s)]^{1/2} \quad \beta = [a/(a + 2s)]^{1/2} \quad \rho = (1 - r)/(1 + r); \quad (3)$$

$\beta$  is also given by

$$\beta = (1 - R_\infty)/(1 + R_\infty)$$

where  $R_\infty$  is the reflectivity of a very thick screen with no light transmission through it,  $a$  and  $s$  are the coefficients of light absorption and light scattering within the phosphor material, and  $r$  is the light reflectivity at the screen–silica substrate interface; reflectivity at the screen–air interface was considered to be approximately zero.  $A_Q$ ,  $n_c$ , and  $G_L$  determine the image brightness produced at a given dose burden to the patient.  $G_L$  is additionally related to the spread of light directed towards the screen output, thus affecting spatial resolution of image receptors. AE in relation (1) has no dimensions. For the calculated AE to be compatible with the experimental results it has to be multiplied by a factor  $\gamma(E) = [\Psi(E)/X(E)]$  (Hendee 1970), converting energy fluence  $\Psi(E)$  into exposure  $X(E)$ .

Since x-ray beams used in radiography are polychromatic, the absolute efficiency was calculated by averaging over the whole x-ray energy spectrum:

$$AE = \left( \int_0^{E_0} AE(E)N_x(E) dE \right) \left( \int_0^{E_0} N_x(E) dE \right)^{-1} \quad (4)$$

where  $E_0$  is the maximum x-ray spectral energy (numerically equal to the tube voltage in kVp) and  $N_x(E)$  is the x-ray spectral distribution function. The shape of the  $N_x(E)$  function depends on the x-ray tube target material, the tube high voltage, and the type of filter material. For most calculations the following relation, which holds for tungsten (W) target tubes (Storm 1972), was employed:

$$N_x(E) = (1 - E/E_0) \exp(-\mu_{Al}d_{Al}) \quad (5)$$

where  $d_{Al}$  is the total aluminum thickness (2 mm x-ray tube filter and 20 mm filter used for simulating x-ray attenuation by human tissues), and  $\mu_{Al}$  is the x-ray attenuation coefficient of aluminum (Storm and Israel 1967). Equation (5) does not account for W K characteristic

x-rays but in our experiments (W target–22 mm Al total filter) their contribution has been shown to be minimal (Cavouras *et al* 1996). However, for calculations concerning mammographic applications a molybdenum (Mo) target model (Tucker *et al* 1991b) that includes the K characteristic lines of Mo was used (see appendix B).

The parameters  $n_c$ ,  $\sigma$ ,  $\beta$ ,  $\rho$ ,  $R_\infty$ ,  $r$ ,  $a$  and  $s$  employed in the above formulas (1) and (3) were determined as follows: the conversion efficiency  $n_c$  and the light attenuation parameter  $\sigma$  (usually called the reciprocal of the light quantum diffusion length (Swank 1973)) were found by fitting equation (4) to absolute efficiency experimental data; fitting was performed by means of the Levenberg–Marquard method (Press *et al* 1989).  $R_\infty$  and  $r$  were experimentally determined by reflectivity measurements performed according to Ludwig (1971) and  $\rho$ ,  $\beta$ ,  $a$  and  $s$  were calculated by equations (3).

## 2.2. Coupling efficiency to optical detectors

In digital x-ray radiographic systems the phosphor screen is optically coupled to a high-sensitivity CCD array by means of fibre optic tapers or optical lenses (Karellas *et al* 1992, Gurwich 1995, Maidment and Yaffe 1995). In such configurations the x-ray to electron conversion efficiency  $N_e(E, T)$ , expressing the number of electrons generated in the optical detector per incident x-ray quantum and for monoenergetic x-rays, is given by

$$N_e(E, T) = A_Q(E, T)m_0(E)G_L(\sigma, \beta, \rho, E, T)C_e \quad (6)$$

where  $m_0(E)$  is the mean number of light photons created per x-ray quantum detected in the phosphor material:

$$m_0(E) = n_c \varepsilon(E) \quad (7)$$

where  $\varepsilon(E)$  is the number of light photons generated when the total energy  $E$  of one x-ray photon is converted into light (i.e.  $n_c = 1$ ):

$$\varepsilon(E) = E \left[ \left( \int_{E_{\lambda_2}}^{E_{\lambda_1}} S_p(E_\lambda) E_\lambda dE_\lambda \right) \left( \int_{E_{\lambda_2}}^{E_{\lambda_1}} S_p(E_\lambda) dE_\lambda \right)^{-1} \right]^{-1} \quad (8)$$

where,  $E_\lambda$  is the energy of optical photons and  $S_p(E_\lambda)$  is the emission spectrum of the screen. The term in square brackets in (8) evaluates the average optical photon energy.  $C_e$  is the optical coupling efficiency, expressing the number of electrons generated in the CCD array per light photon emitted by the screen:

$$C_e = a_s C_l \eta_{\text{CCD}} \quad (9)$$

where  $a_s$  is the spectral matching factor (Giakoumakis 1991, Panayiotakis *et al* 1996), expressing the compatibility between the phosphor's emission spectrum and the spectral sensitivity of the CCD array,  $C_l$  is the light collection efficiency of the optics between the screen and the CCD array, and  $\eta_{\text{CCD}}$  is the intrinsic quantum conversion efficiency of the CCD array in number of electrons generated per incident light photon.  $C_l$  ( $C_l = 0.08$  for fibre optics taper) and  $\eta_{\text{CCD}}$  ( $\eta_{\text{CCD}} = 0.6$ ) were obtained from published data (Gurwich 1995, Karellas *et al* 1992) and  $a_s$  was calculated according to the formula

$$a_s = \left( \int_{\lambda_1}^{\lambda_2} S_p(\lambda) S_d(\lambda) d\lambda \right) \left( \int_{\lambda_1}^{\lambda_2} S_d(\lambda) d\lambda \right)^{-1} \quad (10)$$

where  $\lambda_1$  and  $\lambda_2$  are the lower and upper wavelength limits of the spectrum,  $S_p(\lambda)$  is the normalized spectrum of the phosphor screen, experimentally determined with an Oriel 7240 grating monochromator and  $S_d(\lambda)$  is the normalized spectral sensitivity distribution of the optical detector, obtained from the manufacturer's data (RS Opto-Devices, data sheet 2135,

1981). The spectral matching factor of ZnSCdS:Ag with some commercial radiographic films (Agfa Curix Ortho GS, Kodak X-omatic GR, Fuji UM-MH) employed in conventional rare earth radiographic cassettes was also calculated, even though these films are principally designed for terbium-activated rare earth emission spectra. Parameters  $a_s$ ,  $C_l$  and  $\eta_{\text{CCD}}$  contribute to the sensitivity of a digital detector, thus affecting radiation dose to the patient.

From equations (6) and (7) the electron conversion efficiency  $N_e(E, T)$  can also be expressed in terms of the absolute efficiency as follows:

$$N_e(E, T) = AE(E, T)\varepsilon(E)C_e. \quad (11)$$

$N_e$  is related to patient dose, being a measure of detector sensitivity.  $N_e$  was calculated for screens of coating thicknesses 80 and 35 mg cm<sup>-2</sup> corresponding to those employed in digital radiography and digital mammography respectively.

### 2.3. Image information transfer efficiency

To assess the quality of the radiographic image produced by the ZnSCdS:Ag, Gd<sub>2</sub>O<sub>2</sub>S:Tb, and Y<sub>2</sub>O<sub>2</sub>S:Tb screens, the MTF, the QNTF and the zero-frequency DQE were evaluated. MTF is a function describing the efficiency of signal transfer as a function of spatial frequency and it is indicative of image sharpness and spatial resolution deterioration from the input to the output of an imaging system. QNTF expresses the x-ray quantum noise transfer from input to output as a function of spatial frequency and it is associated with quantum noise content in the resulting radiographic image. DQE(0) expresses the degradation of signal to noise ratio (SNR) from input to output and it is indicative of image information content (Dick and Motz 1981). MTF, QNTF, and DQE(0) were determined considering that the phosphor screen is divided into a number of consecutive thin fluorescent layers (Nishikawa and Yaffe 1990, Van Metter and Rabbani 1990). Calculations of image transfer characteristics were performed under either general radiographic conditions, using a W target x-ray spectrum, or under mammographic conditions, using an Mo x-ray spectrum.

**2.3.1. The modulation transfer function.** The fraction of spatial frequency dependent light flux generated in the phosphor material at depth  $t$  and transmitted to the screen output is given as a function of the previously measured optical parameters  $\sigma$ ,  $\beta$  and  $\rho$  (Ludwig 1971, Swank 1973, Beutel *et al* 1993):

$$G_t(v, t) = \frac{\sigma\rho[(q\beta + \sigma)e^{qT} + (q\beta - \sigma)e^{-qt}]}{(q\beta + \sigma)(q\beta + \sigma\rho)e^{qT} - (q\beta - \sigma)(q\beta - \sigma\rho)e^{-qT}} \quad (12a)$$

for light quanta emitted at the screen surface opposing that of the x-ray beam incidence (transmission mode), and by (Nishikawa and Yaffe 1988)

$$G_r(v, t) = \frac{\sigma\rho[(q\beta + \sigma)e^{q(T-t)} + (q\beta - \sigma)e^{-q(T-t)}]}{(q\beta + \sigma)(q\beta + \sigma\rho)e^{qT} - (q\beta - \sigma)(q\beta - \sigma\rho)e^{-qT}} \quad (12b)$$

for light quanta exiting the screen surface receiving the incident x-ray beam (reflection mode).

$q$  in relations (12) is an optical parameter defined as

$$q = (\sigma^2 + 4\pi^2[v/d]^2)^{1/2} \quad (13)$$

where  $v$  is the spatial frequency and  $d$  is the density of the ZnSCdS:Ag phosphor coating measured in powder form ( $d = 2.71$  g cm<sup>-3</sup>). The measured value of  $d$  corresponds to a packing density of 50.6%, which is similar to that of commercial screens (Zweig and Zweig 1983).

Considering the mean number  $m_0(E)$  of optical photons (see equation (7)) created by an absorbed x-ray quantum, then the product  $m_0(E)G(v, t)$  expresses the mean number of optical photons, generated by an absorbed x-ray quantum in a thin layer at depth  $t$ , that finally escape the screen. The mean number of optical photons emitted by the screen per absorbed x-ray quantum is then computed by averaging the individual layer contributions over the total number of screen layers. This is achieved by multiplying the mean number of optical photons per x-ray  $m_0(E)G(v, t)$  by the number of x-rays absorbed by a thin layer at depth  $t$  and dividing by the total number of x-rays absorbed by the screen. This is equivalent to multiplying by a weighting factor  $X(E, t)$ , representing the fraction of x-rays absorbed by a particular layer  $\mu(E) \exp[-\mu(E)t]$  at depth  $t$  with respect to the total x-ray absorption in the screen  $\int_0^T \mu(E) \exp[-\mu(E)t] dt$ . This factor is given by

$$X(E, t) = \mu(E) \exp[-\mu(E)t] \left( \int_0^T \mu(E) \exp[-\mu(E)t] dt \right)^{-1}. \quad (14)$$

Overall, the mean number of optical photons  $\bar{n}_l(E, v, T)$ , corresponding to contributions from all thin layers, emitted by a phosphor screen of thickness  $T$  per x-ray quantum absorbed within the screen, is given by

$$G(E, v, T) = \int_0^T X(E, t) m_0(E) G(v, t) dt = \bar{n}_l(E, v, T). \quad (15)$$

Considering that the MTF of a thin phosphor layer is

$$\text{MTF}(v, t) = G(v, t)/G(0, t) \quad (16)$$

then relation (15) may be written as

$$\bar{n}_l(E, v, T) = \int_0^T X(E, t) m_0(E) G(0, t) \text{MTF}(v, t) dt. \quad (17)$$

Now, if a fluence  $N_x$  of x-ray quanta is incident on a phosphor screen of thickness  $T$  and detection efficiency  $A_Q$ , then the resulting mean number of emitted light photons is

$$\bar{N}_l(E, v, T) = \bar{n}_x(E, T) \bar{n}_l(E, v, T) \quad (18)$$

where  $\bar{n}_x(E, T)$  is the mean number of absorbed x-ray photons per unit area given by

$$\bar{n}_x(E, T) = \bar{N}_x(E) A_Q(E, T) \quad (19)$$

$\bar{N}_x(E)$  being the mean number of x-ray quanta incident per unit of screen area.

For polyenergetic x-ray beams,  $\bar{N}_x(E)$  represents a differential x-ray spectral fluence  $\bar{N}_x(E) = d\Phi(E)/dE$ , and the total number of optical photons emitted is obtained by integrating over the x-ray spectrum:

$$\bar{N}_l(E_0, v, T) = \int_0^{E_0} \bar{N}_x(E) A_Q(E, T) \int_0^T X(E, t) m_0(E) G(0, t) \text{MTF}(v, t) dt dE \quad (20)$$

where  $E_0$  is the maximum x-ray energy determined by the tube voltage.

The MTF of the screen is then given by

$$\begin{aligned} \text{MTF}(E_0, v, T) &= \frac{\bar{N}_l(E_0, v, T)}{\bar{N}_l(E_0, 0, T)} \\ &= \left( \int_0^{E_0} \bar{N}_x(E) A_Q(E, T) \int_0^T X(E, t) m_0(E) G(0, t) \text{MTF}(v, t) dt dE \right) \\ &\quad \times \left( \int_0^{E_0} \bar{N}_x(E) A_Q(E, T) \int_0^T X(E, t) m_0(E) G(0, t) dt dE \right)^{-1}. \end{aligned} \quad (21)$$

2.3.2. *The quantum noise transfer function.* Quantum noise in a radiographic image is the result of fluctuations in the number of x-ray quanta detected by the screen and of optical photons (optical pulse) emitted per x-ray quantum absorbed. Quantum noise may be expressed in terms of the variance in the number of output light photons  $N_l$  (Dick and Motz 1981):

$$\text{var}(N_l) = \bar{n}_x(E, T) \overline{n_l^2}(E, v, T) \quad (22)$$

where  $\overline{n_l^2}(E, v, T)$  is the mean number of the squares of optical photons  $n_l(E, v, t) = m_0(E)G(v, t)$  generated at each screen thin layer per absorbed x-ray that reach the screen output.  $\overline{n_l^2}(E, v, T)$  is calculated by the product of the fraction of x-rays absorbed at depth  $t$ , which is equal to  $[\mu(E) \exp(-\mu(E)t)]$ , and  $n_l^2(E, v, t)$ , divided by the total fraction of absorbed x-ray photons in the screen, which is equal to  $\int_0^T \mu(E) \exp[-\mu(E)t] dt$ , giving

$$\begin{aligned} \overline{n_l^2}(E, v, T) &= \left( \int_0^T [\mu(E) \exp(-\mu(E)t)] [m_0(E)G(v, t)]^2 dt \right) \\ &\quad \times \left( \int_0^T \mu(E) \exp[-\mu(E)t] dt \right)^{-1} \end{aligned} \quad (23)$$

or making use of relation (14)

$$\overline{n_l^2}(E, v, T) = \int_0^T X(E, t) [m_0(E)G(v, t)]^2 dt. \quad (24)$$

Thus from (19), (22) and (24)

$$\text{var}(N_l) = \bar{N}_x(E) A_Q(E, T) \int_0^T X(E, t) [m_0(E)G(v, t)]^2 dt. \quad (25)$$

However, for polyenergetic beams  $\bar{N}_x(E)$  is represented in terms of the x-ray differential spectral fluence defined in (5) and integrating over the x-ray spectrum equation (25) becomes

$$\text{var}(N_l) = \int_0^{E_0} \bar{N}_x(E) A_Q(E, T) \int_0^T X(E, t) [m_0(E)G(v, t)]^2 dt dE = \text{QN}(E_0, v, T). \quad (26)$$

The quantum noise transfer function (QNTF) is defined as

$$\begin{aligned} \text{QNTF}(E_0, v, T) &= \left[ \frac{\text{QN}(E_0, v, T)}{\text{QN}(E_0, 0, T)} \right]^{1/2} \\ &= \left[ \left( \int_0^{E_0} \bar{N}_x(E) A_Q(E, T) \int_0^T X(E, t) [m_0(E)G(v, t)]^2 dt dE \right) \right. \\ &\quad \left. \times \left( \int_0^{E_0} \bar{N}_x(E) A_Q(E, T) \int_0^T X(E, t) [m_0(E)G(0, t)]^2 dt dE \right)^{-1} \right]^{1/2} \end{aligned} \quad (27)$$

expressing the quantum noise propagation through the screen, which is analogous to the signal propagation efficiency MTF( $E_0, v, T$ ).

From equations (16) and (27) it can be seen that QNTF( $E_0, v, T$ ) squared is a weighted sum of the individual thin-layer MTFs squared, which is equivalent to the normalized quantum noise power spectrum (Nishikawa and Yaffe 1990).

2.3.3. *The detective quantum efficiency.* The zero-spatial-frequency DQE is defined (Dainty and Shaw 1974, Swank 1974, Dick and Motz 1981) as the ratio

$$\text{DQE}(0) = [\text{SNR}_{out}/\text{SNR}_{in}]^2 \quad (28)$$

where  $\text{SNR}_{out}$  and  $\text{SNR}_{in}$  are the output and input signal to noise ratios respectively. The input signal to noise ratio is defined as

$$\text{SNR}_{in}^2 = [\bar{N}_x(E)]^2/\text{var}[N_x(E)] \quad (29)$$

where  $\bar{N}_x(E)$ , defined in (19), represents the input signal and  $\text{var}(N_x)$  is the variance in the number of incident x-ray quanta expressing input quantum noise. Assuming Poisson statistics for the x-ray photons,

$$\text{var}[N_x(E)] = \bar{N}_x(E) \quad (30)$$

thus

$$\text{SNR}_{in}^2 = \bar{N}_x(E). \quad (31)$$

Regarding the output signal to noise ratio:

$$\text{SNR}_{out}^2 = [\bar{N}_l(E, 0, T)]^2/\text{var}[N_l(E, 0, T)] \quad (32)$$

where  $\bar{N}_l(E, 0, T)$  is the mean value of output light photons defined in (20) at  $v = 0$ , representing the output signal. From equations (15), (18), and (19) the output signal is

$$\bar{N}_l(E, 0, T) = \bar{n}_x(E, T)\bar{n}_l(E, 0, T) = \bar{N}_x(E)A_Q(E, T) \int_0^T X(E, t)m_0(E)G(0, t) dt. \quad (33)$$

Therefore, from (25) and (33) at  $v = 0$

$$\begin{aligned} [\text{SNR}_{out}]^2 &= \left( \bar{N}_x(E)A_Q(E, T) \left[ \int_0^T X(E, t)m_0(E)G(0, t) dt \right]^2 \right) \\ &\quad \times \left( \int_0^T X(E, t)[m_0(E)G(0, t)]^2 dt \right)^{-1} \end{aligned} \quad (34)$$

and

$$\begin{aligned} \text{DQE}(E, 0, T) &= A_Q(E, T) \left[ \int_0^T X(E, t)m_0(E)G(0, t) dt \right]^2 \\ &\quad \times \left( \int_0^T X(E, t)[m_0(E)G(0, t)]^2 dt \right)^{-1} \end{aligned} \quad (35)$$

or

$$\text{DQE}(E, 0, T) = A_Q(E, T)[M_1(E, T)]^2/M_2(E, T) \quad (36)$$

where

$$M_n(E, T) = \int_0^T X(E, t)[m_0(E)G(0, t)]^n dt \quad (37)$$

for  $n = 1, 2$  are called the first and second monoenergetic moments of the statistical distribution of the emitted optical pulses (light photons per absorbed x-ray quantum).  $M_1$  is related to the mean value (see equation (17)) and  $M_2$  to the variance (see equations (24) and (25)) of the magnitudes of the emitted optical pulses. Thus,  $\text{DQE}(E, 0, T)$  can be written as

$$\text{DQE}(E, 0, T) = A_Q(E, T)A_S(E, T) \quad (38)$$

where

$$A_S(E, T) = [M_1(E, T)]^2 / M_2(E, T). \quad (39)$$

$A_S(E, T)$  is called the Swank factor or statistical factor (Swank 1973, 1974, Dick and Motz 1981) and is associated with the statistical fluctuations in the number of optical photons emitted by the screen per absorbed x-ray quantum.

For polyenergetic x-ray beams DQE is calculated by averaging  $A_Q$ ,  $M_1$  and  $M_2$  separately (Swank 1974) over the x-ray spectrum using relations (2) and (37) respectively

$$A_Q(E_0, T) = \left( \int_0^{E_0} \bar{N}_x(E) \int_0^T (1 - \exp[-\mu(E)T]) dt dE \right) \left( \int_0^{E_0} \bar{N}_x(E) dE \right)^{-1} \quad (40)$$

$$M_n(E_0, T) = \left( \int_0^{E_0} \bar{N}_x(E) \int_0^T X(E, t) [m_0(E)G(0, t)]^n dt dE \right) \left( \int_0^{E_0} \bar{N}_x(E) dE \right)^{-1}. \quad (41)$$

For incident x-ray energies just exceeding the K absorption edges of Gd ( $E_K = 50.2$  keV), Cd ( $E_K = 26.7$  keV), and Y ( $E_K = 17$  keV), the production of fluorescent K characteristic x-rays within the three phosphor materials must be taken into account. Corresponding corrections were performed following methods described by Chan and Doi (1983) and Fahrig *et al* (1995).

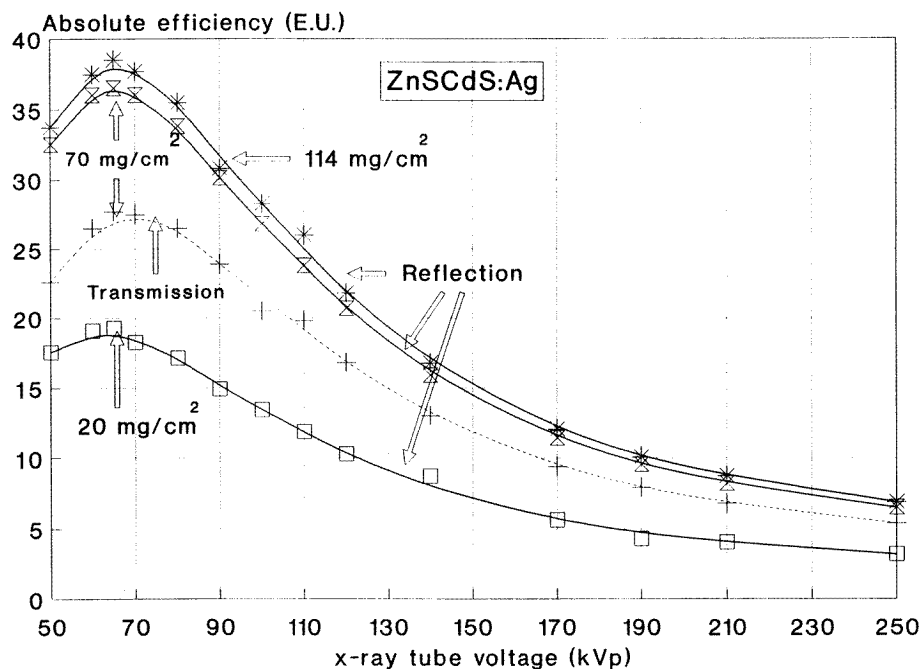


**Figure 1.** The variation of AE with tube voltage for three ZnSCdS:Ag laboratory-prepared screens of coating thicknesses 20, 70, and 114 mg cm<sup>-2</sup> measured in reflection mode; the 70 mg cm<sup>-2</sup> screen is also presented in transmission mode. Points, experimental values; lines, theoretical curves. (1 efficiency unit, 1 EU = 1 μW m<sup>-2</sup> (mR s<sup>-1</sup>)<sup>-1</sup> or 3.875 J (C kg<sup>-1</sup> m<sup>2</sup>)<sup>-1</sup> SI units.)

### 3. Results and discussion

The variation of absolute efficiency with tube voltage in reflection mode is shown in figure 1 for three ZnSCdS:Ag screens of 20, 70 and 114 mg cm<sup>-2</sup>. In the same figure data obtained in transmission mode are also included for the 70 mg cm<sup>-2</sup> screen. Curves were calculated employing the theoretical model of equations (4) and (A3) and (A4) of appendix A. Optimum values for  $n_c$  and  $\sigma$  were  $n_c = 0.207$  and  $\sigma = 33.8$  cm<sup>2</sup> g<sup>-1</sup>. The value of x-ray to light conversion efficiency ( $n_c$ ) is close to that reported by Ludwig ( $n_c = 0.211$ ; Ludwig 1971), and exceeds the high  $n_c$  values of terbium-activated phosphors Gd<sub>2</sub>O<sub>2</sub>S:Tb ( $n_c = 0.20$ ), Y<sub>2</sub>O<sub>2</sub>S:Tb ( $n_c = 0.18$ ), and La<sub>2</sub>O<sub>2</sub>S:Tb ( $n_c = 0.18$ ) often used in medical radiography (Giakoumakis *et al* 1990, Kandarakis *et al* 1996). The value of  $n_c$  for ZnSCdS:Ag is also higher than those of other phosphors commercially used in radiography such as CaWO<sub>4</sub> ( $n_c = 0.035$ ), BaSO<sub>4</sub>:Pb ( $n_c = 0.04$ ), BaSO<sub>4</sub>:Eu ( $n_c = 0.08$ ), and CsI:Na ( $n_c = 0.10$ ) employed in the input screen of image intensifiers (Arnold 1979).

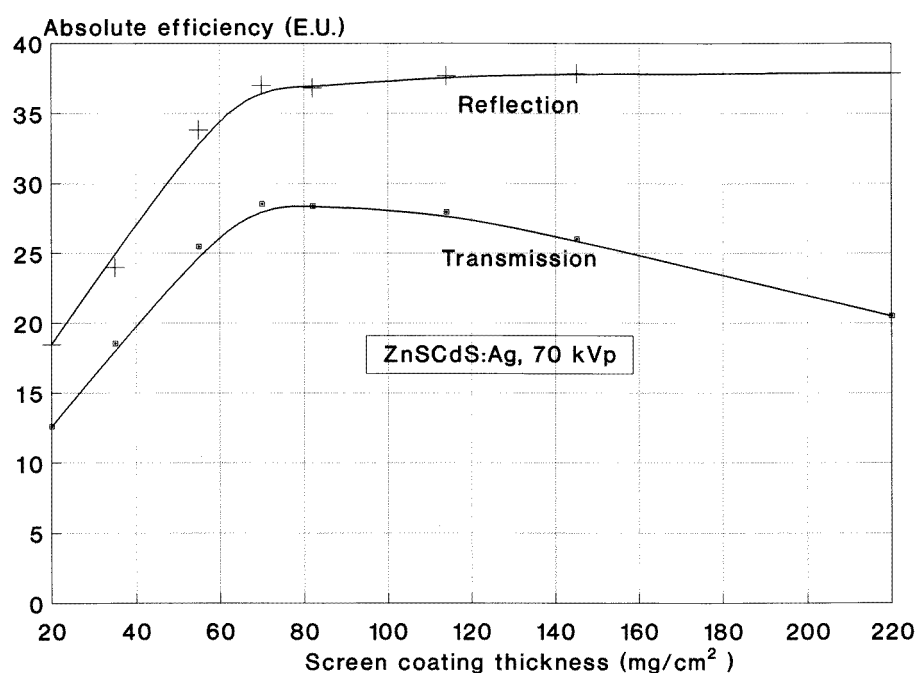


**Figure 2.** The variation of AE of ZnSCdS:Ag screens with coating thickness in transmission and reflection modes at 70 kVp: points, experimental values; solid lines, theoretical curves. (1 efficiency unit, 1 EU = 1  $\mu\text{W m}^{-2}$  (mR s<sup>-1</sup>)<sup>-1</sup> or 3.875 J (C kg<sup>-1</sup> m<sup>2</sup>)<sup>-1</sup> SI units).

Peak values of absolute efficiency in reflection mode of measurement were obtained at 65 kVp. The peak AE values corresponding to the screens shown are 18.829, 36.507, and 38.025 efficiency units (EU) (1 EU = 1  $\mu\text{W m}^{-2}$  (mR s<sup>-1</sup>)<sup>-1</sup> or 3.875 J (C kg<sup>-1</sup> m<sup>2</sup>)<sup>-1</sup>, expressed in SI units) for the 20, 70 and 114 mg cm<sup>-2</sup> ZnSCdS:Ag screens respectively. It is observed that AE is rapidly decreasing after 80 kVp resulting in a drop of about 13 EU ( $\approx 34\%$ ) between 65 and 110 kVp for the 114 mg cm<sup>-2</sup> screen. This is because ZnSCdS has a low effective atomic number, thus absorption of higher-energy x-rays by the phosphor material is relatively reduced. Additionally, in the reflection mode of measurement, deeper

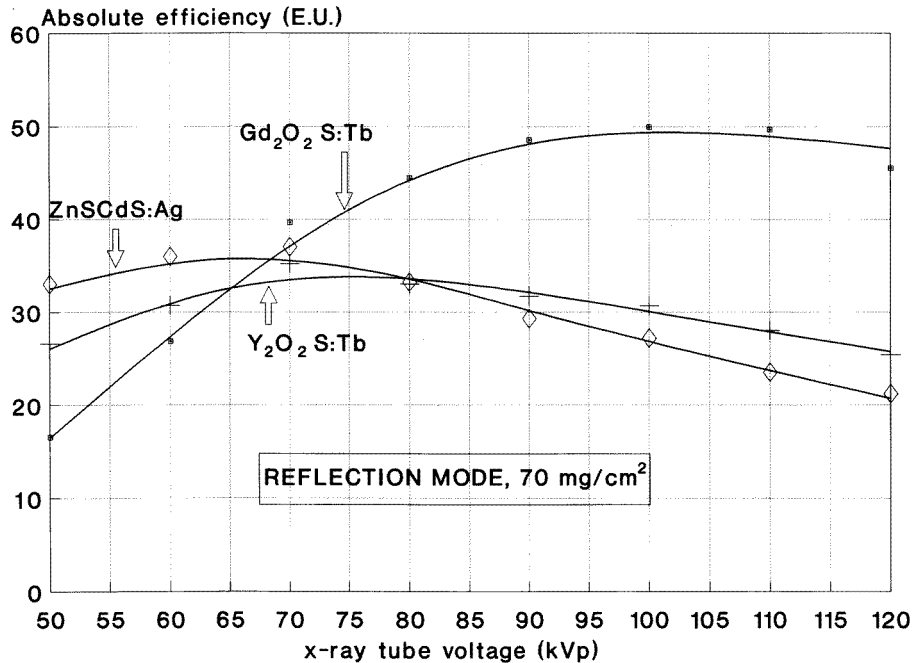


**Figure 3.** Absolute efficiencies in reflection mode versus tube voltage for 70 mg cm<sup>-2</sup> ZnSCdS:Ag, Gd<sub>2</sub>O<sub>2</sub>S:Tb, and Y<sub>2</sub>O<sub>2</sub>S:Tb phosphor screens: points, experimental values; solid lines, theoretical curves. (1 efficiency unit, 1 EU = 1 μW m<sup>-2</sup> (mR s<sup>-1</sup>)<sup>-1</sup> or 3.875 J (C kg<sup>-1</sup> m<sup>2</sup>)<sup>-1</sup> SI units.)

penetration of high-energy x-rays in the phosphor material lengthens the optical photon trajectories towards the emitting surface, thus increasing light attenuation. However, light fluxes in the region of 50–80 kVp ( $\approx$ 30–55 keV mean x-ray energy) are high enough for most radiographic techniques (70–80 kVp for abdominal imaging, 65–75 kVp for lumbar spine radiography, 55–65 kVp for cranial radiography, 60–70 kVp for abdominal angiography). It is also observed that throughout the whole kVp range AE is higher in reflection mode than in transmission mode with a tendency to converge at higher voltages. At high tube voltages the increased depth of x-ray penetration causes the optical photon paths to lengthen in reflection mode but to shorten in transmission mode for a given screen thickness. Thus, absolute efficiencies tend to converge at high voltages.

Figure 2 shows the variation of AE with screen thickness at 70 kVp. Absolute efficiency in reflection mode is superior for the whole screen thickness range and after reaching a plateau level of about 37 EU at 70 mg cm<sup>-2</sup> it remains relatively constant thereafter. This is because x-rays are mostly absorbed close to the exposed surface. Thus, in the reflection mode of measurement light photons travel shorter distances to reach the emitting surface, suffering lower attenuation. As screen thickness increases the depth of x-ray absorption increases up to a maximum over which very few new x-ray photons are absorbed. Therefore, the maximum depth at which optical photons originate remains approximately constant, giving rise to the flat region of AE after 70 mg cm<sup>-2</sup>. In contrast, in transmission mode increasing screen thickness implies longer light photon trajectories before reaching the screen emitting surface, resulting in diminishing output light fluxes. It is important to note that maximum AE is attained at relatively low coating thickness (70 mg cm<sup>-2</sup>), ensuring satisfactory spatial resolution.

In figure 3 efficiency data for the terbium-activated phosphor materials  $\text{Gd}_2\text{O}_2\text{S:Tb}$  and  $\text{Y}_2\text{O}_2\text{S:Tb}$  are plotted against corresponding  $\text{ZnSCdS:Ag}$  data; all screens were prepared and measured by the same method and had approximately the same thickness of  $70 \text{ mg cm}^{-2}$ .  $\text{ZnSCdS:Ag}$  is better than either  $\text{Gd}_2\text{O}_2\text{S:Tb}$  or  $\text{Y}_2\text{O}_2\text{S:Tb}$  up to about 70 or 80 kVp respectively and it remains close to  $\text{Y}_2\text{O}_2\text{S:Tb}$  thereafter. However, the supremacy of  $\text{Gd}_2\text{O}_2\text{S:Tb}$  over the other two phosphors above 80 kVp is impressive, while equally promising is the  $\text{ZnSCdS:Ag}$  phosphor for tube voltages lower than 60 kVp.

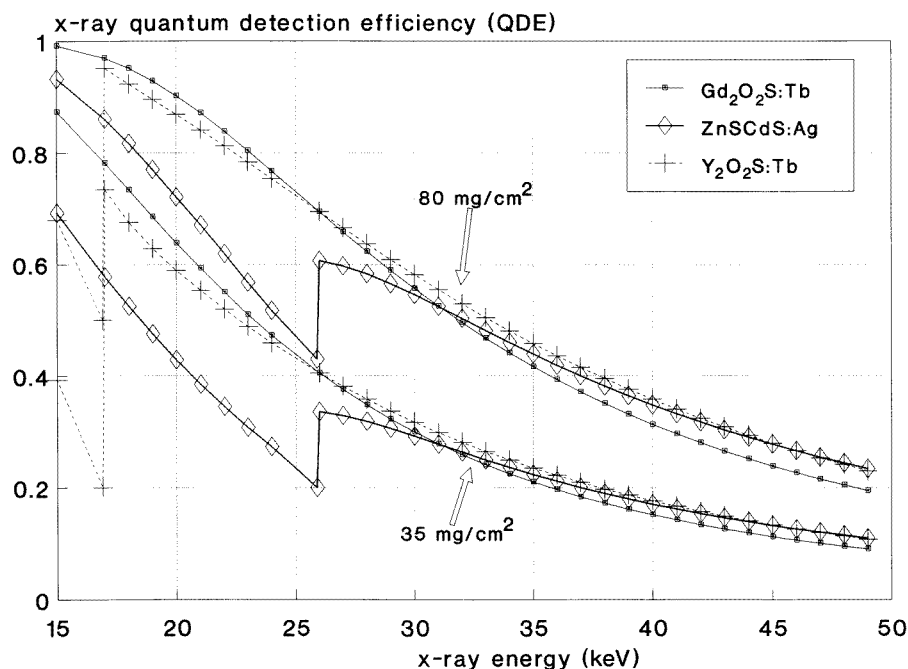


**Figure 4.** Variation of x-ray quantum detection efficiency with x-ray energy for 35 and  $80 \text{ mg cm}^{-2}$   $\text{ZnSCdS:Ag}$ ,  $\text{Gd}_2\text{O}_2\text{S:Tb}$ , and  $\text{Y}_2\text{O}_2\text{S:Tb}$  phosphor screens.

Overall, the absolute efficiency data show that the light output of  $\text{ZnSCdS:Ag}$  is adequately high at dose levels comparable to dose levels required by commercially available phosphors. This is because, although the effective atomic number of  $\text{ZnSCdS:Ag}$  is relatively low,  $\text{ZnSCdS:Ag}$  has the largest intrinsic x-ray to light conversion efficiency ( $n_c$ ) among the phosphors commercially used in radiography. Additionally, the  $\text{ZnSCdS:Ag}$  x-ray detection efficiency ( $A_Q$ ) is comparable to the  $A_Q$  of those phosphors in a region of energies useful for radiography (30–50 keV) above the K edge of Cd at 26.7 keV as shown in figure 4. The light transmission efficiency ( $G_l$ ), mainly determined by the values of intrinsic optical coefficients  $\sigma$  and  $\beta$  of  $\text{ZnSCdS:Ag}$  ( $\sigma = 33.8 \text{ cm}^2 \text{ g}^{-1}$  and  $\beta = 0.04$ ) is also comparable to the transmission efficiencies of the terbium-activated phosphors  $\text{Gd}_2\text{O}_2\text{S:Tb}$ ,  $\text{La}_2\text{O}_2\text{S:Tb}$ , and  $\text{Y}_2\text{O}_2\text{S:Tb}$  ( $\sigma = 30 \text{ cm}^2 \text{ g}^{-1}$  and  $\beta = 0.03$ , being the same for the three phosphors). Values of optical absorption ( $a$ ) and scattering ( $s$ ) coefficients calculated from the above data show that light absorption is higher in  $\text{ZnSCdS:Ag}$  ( $a = 1.5 \text{ cm}^2 \text{ g}^{-1}$  against  $0.9 \text{ cm}^2 \text{ g}^{-1}$  for terbium phosphors) while light scattering is lower ( $s = 377.01 \text{ cm}^2 \text{ g}^{-1}$  against  $499.55 \text{ cm}^2 \text{ g}^{-1}$  for terbium phosphors). Conclusively, radiographic image receptors containing  $\text{ZnSCdS:Ag}$  screens could be employed in most radiographic techniques requiring

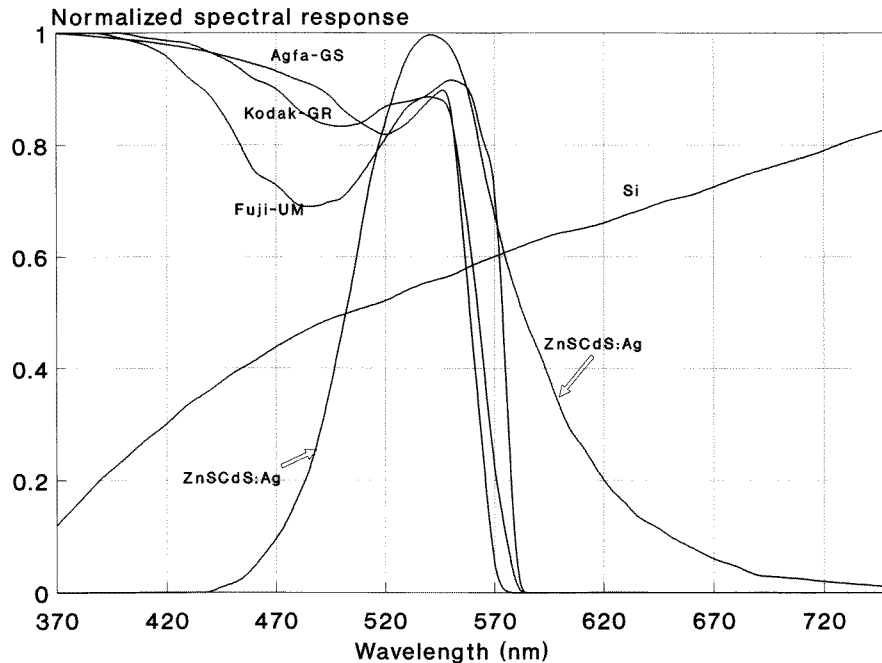


**Figure 5.** Normalized spectral response of the ZnSCdS:Ag phosphor against normalized spectral sensitivities of various optical detectors.

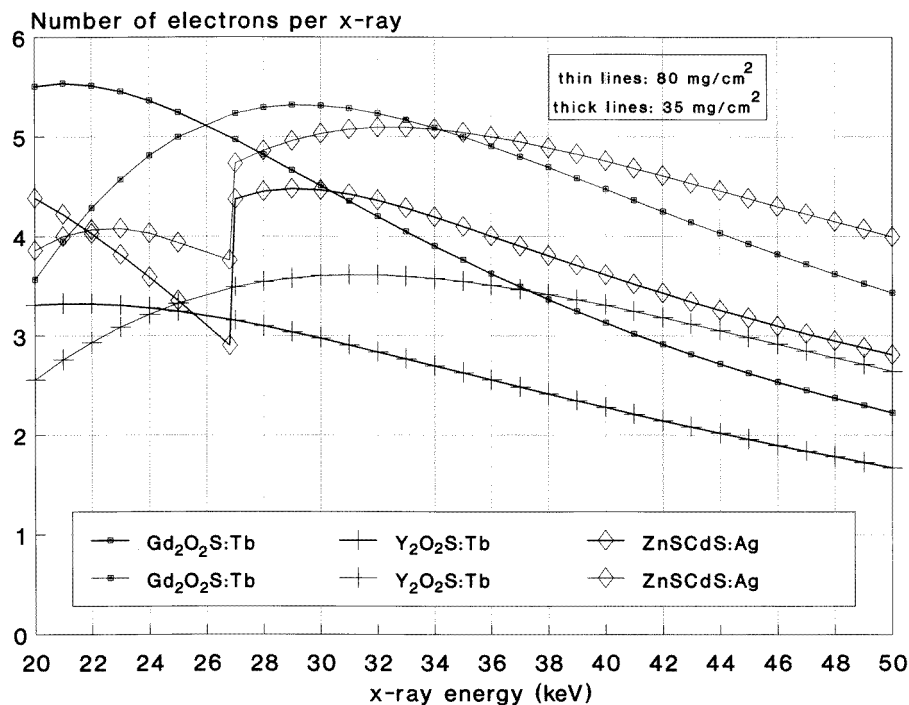
x-ray tube voltages below 80 kVp such as those used for imaging of the abdomen, the lumbar spine, and the cranium. ZnSCdS:Ag can be also used in angiography and probably in mammography, as it can be assessed by extrapolating the ZnSCdS:Ag curve in figure 3 towards lower voltages.

Figure 5 shows the spectrum of ZnSCdS:Ag measured with a monochromator together with the normalized spectral sensitivities of some currently employed commercial x-ray films and an Si photodiode. The latter is used in the CCD arrays of digital radiography systems. Calculated values of spectral matching factors, employing relation (10), are shown in table 1. It is evident that the spectral compatibility of ZnSCdS:Ag with the green sensitive orthochromatic x-ray films (Agfa Curix Ortho GS, Kodak X-omatic GR, Fuji UM-MH) is satisfactory (above 0.5) even though less than those of  $Gd_2O_2S:Tb$  and  $Y_2O_2S:Tb$ . However, these x-ray films have been specifically designed to meet terbium-activated rare earth phosphor spectra. Photographic emulsions with extended spectral sensitivity to match the ZnSCdS:Ag spectrum could be prepared by adding special dyes to enhance spectral compatibility. It is, thus, shown that ZnSCdS:Ag screens combined with orthochromatic films or photodiode arrays might be an efficient radiographic image receptor, especially for tube voltages less than 70 kVp (see figure 3), where the absolute efficiency of ZnSCdS:Ag exceeds the efficiencies of the other phosphor materials. It is noticeable that the matching factor of ZnSCdS:Ag with the Si photodiode, often employed in digital radiography systems, is slightly better than that of  $Gd_2O_2S:Tb$ , which is the phosphor mostly used in these systems (Karellas *et al* 1992, Gurwich 1995, Maidment and Yaffe 1995).

Figure 6 displays results concerning the number of electrons generated in the optical detector (CCD) of a digital imaging system per x-ray photon incident on the phosphor screen

**Table 1.** Spectral matching factors.

Optical detector	ZnSCdS:Ag	Gd <sub>2</sub> O <sub>2</sub> S:Tb	Y <sub>2</sub> O <sub>2</sub> S:Tb
GaAs photocathode	0.942	0.939	0.927
Si photodiode	0.572	0.543	0.411
Agfa Curix Ortho GS radiographic film	0.571	0.692	0.827
Kodak X-omatic GR radiographic film	0.541	0.701	0.833
Fuji UM-MH radiographic film	0.613	0.698	0.802

**Figure 6.** Number of electrons  $N_e$  in the Si photodiode versus x-ray energy for 35 and 80 mg cm<sup>-2</sup> ZnSCdS:Ag, Gd<sub>2</sub>O<sub>2</sub>S:Tb, and Y<sub>2</sub>O<sub>2</sub>S:Tb phosphor screens.

(see equation (6)). The variation in the number of electrons per x-ray ( $N_e$ ) with x-ray energy is shown for three 35 mg cm<sup>-2</sup> and for three 80 mg cm<sup>-2</sup> phosphor screens, simulating screens used in mammography and general radiography respectively. For energies above 30 keV for the 35 mg cm<sup>-2</sup> screens or above 34 keV for the 80 mg cm<sup>-2</sup> screens, the system utilizing the ZnSCdS:Ag screen is more efficient than the system with the Gd<sub>2</sub>O<sub>2</sub>S:Tb screen employing the same optics to interface the phosphor screen with the CCD detector. Additionally, the electron production efficiency of the ZnSCdS:Ag-Si system is higher in the whole energy range than that of the corresponding Y<sub>2</sub>O<sub>2</sub>S:Tb-Si system. This is in agreement with results shown in figure 3, where the luminescence efficiency of ZnSCdS:Ag is higher for voltages between 50 and 70 kVp ( $\approx$  30–45 keV). ZnSCdS:Ag-Si superiority is also justified because the spectral matching of Si is better with ZnSCdS:Ag than with either Gd<sub>2</sub>O<sub>2</sub>S:Tb or Y<sub>2</sub>O<sub>2</sub>S:Tb (table 1).

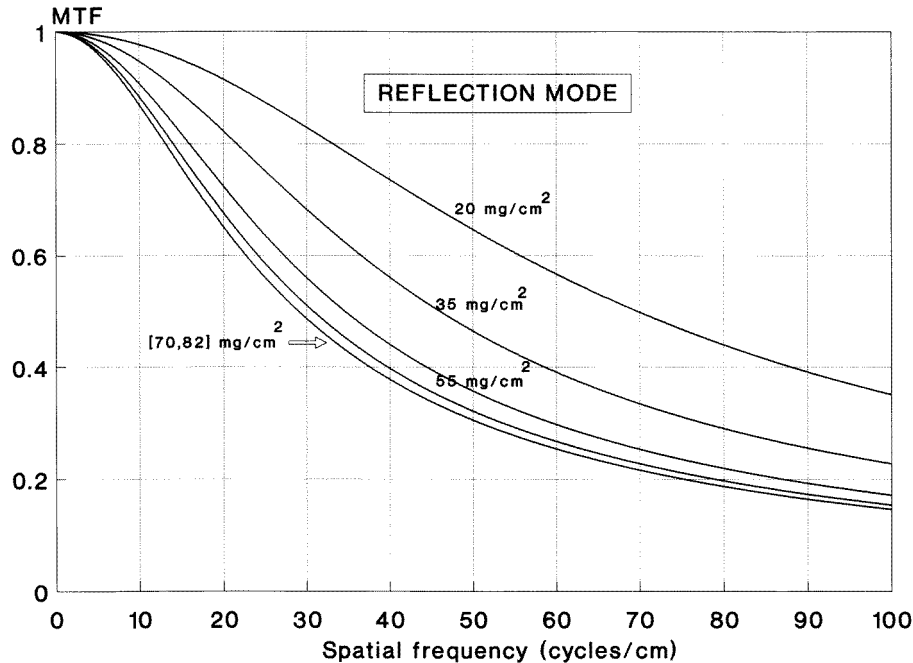


**Figure 7.** MTF curves of ZnSCdS:Ag screens calculated in reflection mode at 70 kVp tube voltage.

Figure 7 shows the MTF curves of several ZnSCdS:Ag screens calculated in reflection mode using the experimentally determined optical parameters  $q$ ,  $\sigma$ ,  $\beta$  and  $\rho$  in equations (12) and (21). It is observed that the MTF curves do not change significantly for screens thicker than  $55 \text{ mg cm}^{-2}$ . Thus, the  $70 \text{ mg cm}^{-2}$  optimum luminescent screen in figure 2 is expected to maintain satisfactory spatial resolution and image sharpness. In figure 8 the MTF curves in reflection mode and transmission mode are compared for a  $35 \text{ mg cm}^{-2}$  ZnSCdS:Ag screen at 25 kVp, using an Mo x-ray spectrum to simulate mammographic conditions, and for an  $80 \text{ mg cm}^{-2}$  ZnSCdS:Ag screen at 70 kVp, using a W x-ray spectrum to simulate general radiographic conditions. At 25 kVp the MTF is better in reflection mode than in transmission mode but these differences are minimized at higher x-ray energies. This finding is important for mammography considering that reflection concerns conventional and transmission digital systems. The reasoning behind differences in the MTFs is similar to that previously given for AEs and holds for all phosphor materials. At low x-ray energies, distances travelled by emitted light quanta within the phosphor are shorter in reflection than in transmission. In the latter, light spread is more extensive, leading to degradation in image sharpness and spatial resolution. At high x-ray energies, x-rays penetrate deeper, transmission mode optical trajectories are shortened, and, thus, differences between the MTFs are not important.

Figure 9 shows a comparison between the MTFs of ZnSCdS:Ag,  $\text{Gd}_2\text{O}_2\text{S:Tb}$ , and  $\text{Y}_2\text{O}_2\text{S:Tb}$  screens, using a 90 kVp W spectrum with  $80 \text{ mg cm}^{-2}$  screen thickness for general radiographic conditions and a 25 kVp Mo spectrum with  $35 \text{ mg cm}^{-2}$  screen thickness for mammographic conditions. Spatial resolution and sharpness of ZnSCdS:Ag are slightly better than those of  $\text{Y}_2\text{O}_2\text{S:Tb}$  but lower than those of  $\text{Gd}_2\text{O}_2\text{S:Tb}$ . These findings

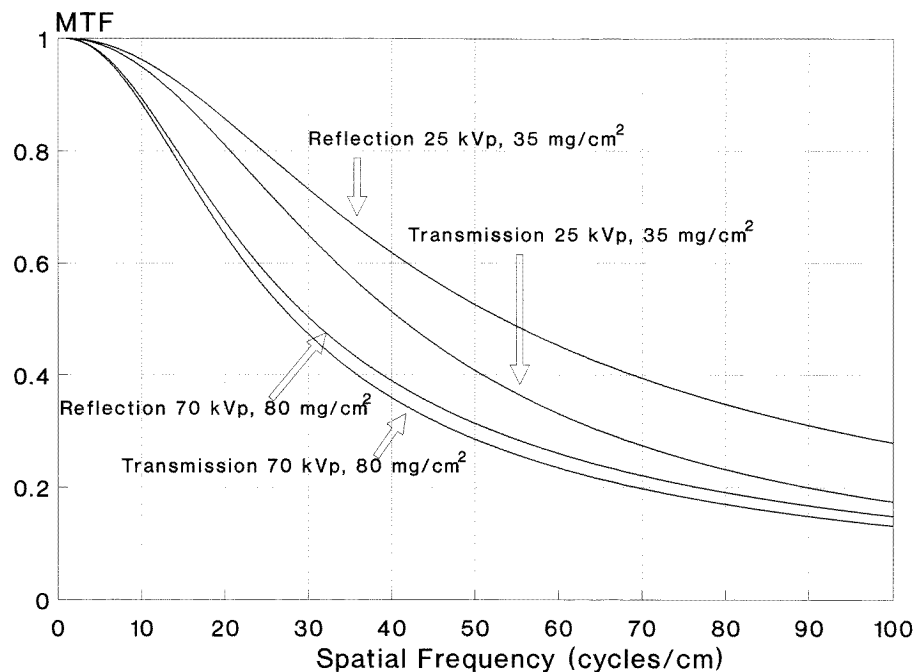


**Figure 8.** MTF curves in reflection and transmission modes for a  $35 \text{ mg cm}^{-2}$  ZnSCdS:Ag screen at 25 kVp (Mo spectrum), and for an  $80 \text{ mg cm}^{-2}$  ZnSCdS:Ag screen at 70 kVp (W spectrum).

may be attributed to deviations in light output at various frequencies, which are due to differences in parameters  $\mu(E)$ ,  $\sigma$  and  $\beta$  between the three materials (see equations (12) and (21)).

Figure 10 shows a comparison between the QNTFs of ZnSCdS:Ag,  $\text{Y}_2\text{O}_2\text{S:Tb}$ , and  $\text{Gd}_2\text{O}_2\text{S:Tb}$  screens, using similar conditions as in the case of MTF. The variation of QNTF with spatial frequency for the three phosphors follows a pattern similar to that of the MTF. This is expected because MTF and QNTF depend on the same optical and x-ray attenuation properties. The QNTF values are higher than the corresponding MTF values, indicating that quantum noise is more efficiently transferred through the screen.

The variation of  $\text{DQE}(0)$  with screen thickness for the ZnSCdS:Ag phosphor is presented in figure 11. Curves have been calculated employing formula (35) for monoenergetic x-ray beams and may be of value in predicting the screen thickness that provides maximum SNR at each x-ray energy.  $\text{DQE}(0)$  was found to be increased at low x-ray energies and at low to medium coating thicknesses. At low energies the quantum detection efficiency ( $A_Q$ ) is significant, giving high  $\text{DQE}(0)$  values in equation (35). At low thicknesses, distances travelled and attenuation suffered by the generated optical pulses are small, thus, emitted optical pulses are of approximately equal magnitudes. This results in narrow optical pulse statistical distributions, which correspond to low values of statistical variance (related to the term in round brackets in equation (35) or  $M_2$  in (36)) inducing high  $\text{DQE}(0)$  values. At higher screen thicknesses, although the x-ray detection efficiency is increased,  $M_2$  is relatively high, because of greater fluctuations in the amplitudes of the emerging optical pulses, thus causing an overall reduction in  $\text{DQE}(0)$ . For energies above the cadmium K absorption edge (26.7 keV), corrections for the K fluorescence effect were performed.

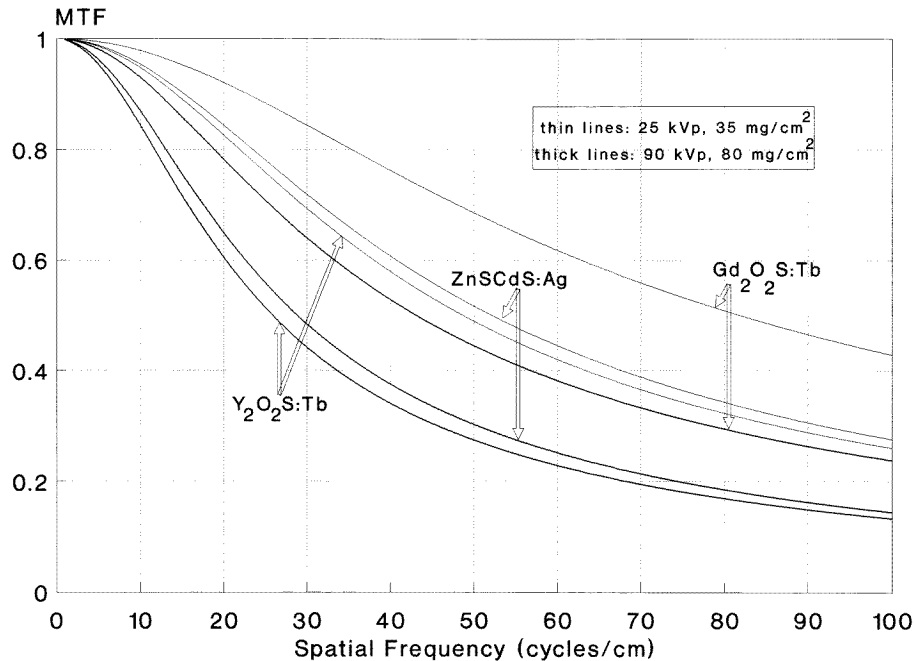


**Figure 9.** MTF curves in reflection mode for  $80 \text{ mg cm}^{-2}$  at 90 kVp (W spectrum) and for  $35 \text{ mg cm}^{-2}$  at 25 kVp (Mo spectrum) ZnSCdS:Ag,  $\text{Gd}_2\text{O}_2\text{S:Tb}$  and  $\text{Y}_2\text{O}_2\text{S:Tb}$  phosphor screens.

The K effect causes reemission of x-rays within the phosphor, which either are absorbed or escape the screen, causing an additional broadening in the statistical distribution of the emitted pulses. This increases  $M_2$ , resulting in reduced  $\text{DQE}(0)$  values. As screen thickness increases, the x-ray quantum detection efficiency is augmented even at high x-ray energies, affecting  $\text{DQE}(0)$ . Thus, the  $\text{DQE}(0)$  at 50 keV is higher than the  $\text{DQE}(0)$  at 15 keV in the thick-screen range. Figure 12 shows the variation of  $\text{DQE}(0)$  with screen thickness for ZnSCdS:Ag,  $\text{Gd}_2\text{O}_2\text{S:Tb}$ , and  $\text{Y}_2\text{O}_2\text{S:Tb}$  screens for the 90 kVp W spectrum and 25 kVp Mo spectrum. The  $\text{DQE}(0)$  of  $\text{Gd}_2\text{O}_2\text{S:Tb}$  is superior in the whole range of coating thicknesses at 90 kVp due to its higher x-ray detection efficiency and its slightly lower value of light attenuation coefficient  $\sigma$ , giving a better optical pulse statistical response. The  $\text{DQE}(0)$  of ZnSCdS:Ag at 25 kVp is slightly higher than that of  $\text{Gd}_2\text{O}_2\text{S:Tb}$  for screen thicknesses thicker than  $80 \text{ mg cm}^{-2}$ . It is also better than that of  $\text{Y}_2\text{O}_2\text{S:Tb}$  at both 90 kVp and 25 kVp principally due to its higher x-ray to light conversion efficiency, producing larger number of optical photons ( $m_0$ ) per x-ray detected. This increases the mean value of the optical pulse statistical distribution and, thus, the first moment  $M_1$  in equation (36), resulting in higher  $\text{DQE}(0)$ .

To test the validity of our calculations, published experimental data on MTF (Desponds *et al* 1991, Bunch *et al* 1987) and QNTF (Nishikawa and Yaffe 1988) of a commercial screen (Kodak Min-R,  $31.7 \text{ mg cm}^{-2}$   $\text{Gd}_2\text{O}_2\text{S:Tb}$ ) were compared with our results as shown in figure 13. Satisfactory agreement was obtained by using in our MTF and QNTF calculations as reflectivity values for the Kodak Min-R screen those reported by Nishikawa and Yaffe (1988) ( $\rho = 0.8$  and  $\rho = 0.25$  for screen-film and screen-substrate interfaces respectively),

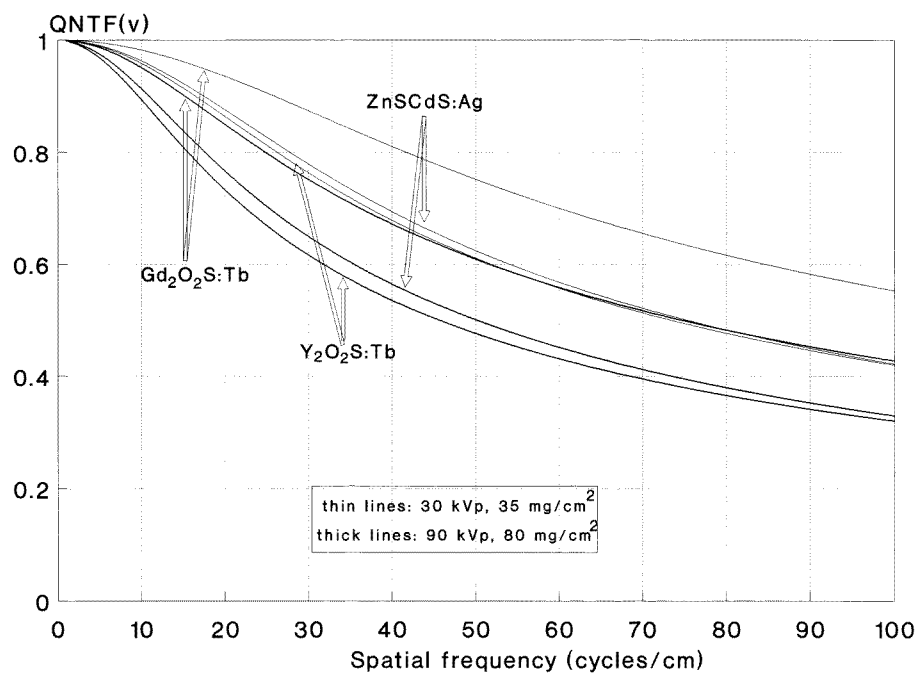


**Figure 10.** QNTF curves in reflection mode for  $80 \text{ mg cm}^{-2}$  at 90 kVp (W spectrum) and for  $35 \text{ mg cm}^{-2}$  at 30 kVp (Mo spectrum) ZnSCdS:Ag, Gd<sub>2</sub>O<sub>2</sub>S:Tb, and Y<sub>2</sub>O<sub>2</sub>S:Tb phosphor screens.

since, to our knowledge, the exact reflectivity values are not available from the manufacturer. Using different values for optical parameters is justified because some of the commercial screen characteristics such as screen substrate, grain size and shape, binding material, and light absorbing dyes, most probably differ or are not present in our laboratory-prepared screens. Also the validity of our DQE(0) calculations was tested against published DQE(0) data for the Kodak Min-R screen (Fahrig *et al* 1995): at 30 keV, the DQE(0) of the Kodak Min-R screen was approximately 0.2 against 0.23 found by our method for a Gd<sub>2</sub>O<sub>2</sub>S:Tb screen of approximately the same thickness. From 40 to 49 keV, our results were practically identical to those of the commercial screen ( $\text{DQE}(0)_{40} = 0.11$  and  $\text{DQE}(0)_{49} = 0.07$ ).

#### 4. Summary and conclusions

ZnSCdS:Ag laboratory prepared phosphor screens were evaluated under radiographic conditions and were compared to similarly prepared Gd<sub>2</sub>O<sub>2</sub>S:Tb and Y<sub>2</sub>O<sub>2</sub>S:Tb phosphor screens. The evaluation comprised (i) the measurement of the x-ray luminescence efficiencies and of the optical emission spectra, (ii) the determination of optical parameters related to light generation and attenuation within the phosphor material and of phosphor coupling efficiencies to radiographic optical photon detectors, and (iii) the calculation of image transfer properties described by MTF, QNTF, and DQE.

ZnSCdS:Ag was found adequately efficient for radiographic applications displaying the highest intrinsic x-ray to light conversion efficiency. Its coupling efficiencies to common

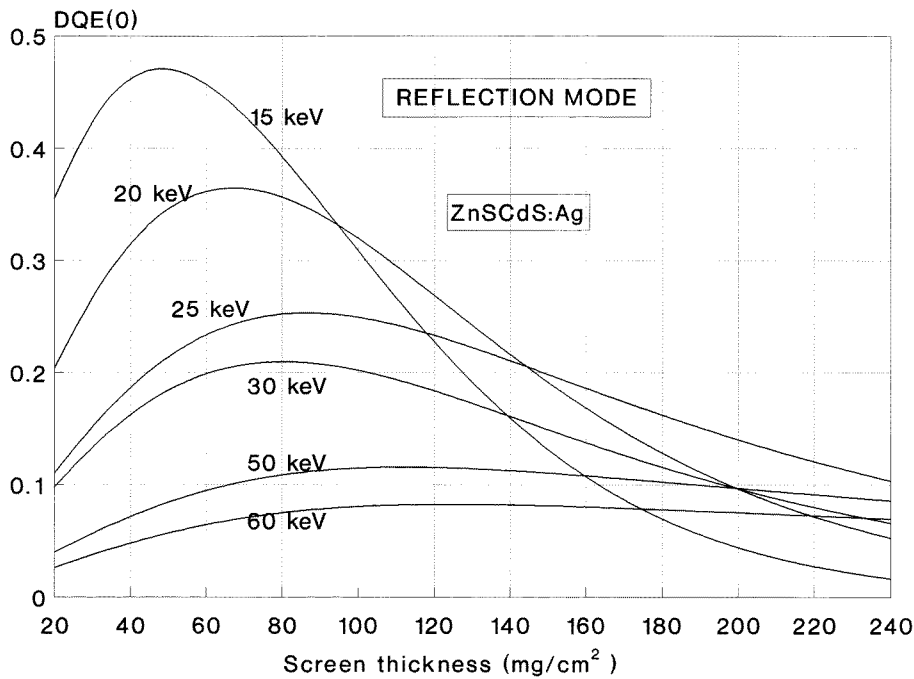


**Figure 11.** Zero-frequency detectable quantum efficiency (DQE(0)) of ZnSCdS:Ag versus screen coating thickness at various x-ray energies.

films and to the Si photodiode were satisfactory while its image transfer characteristics were better than those of  $Y_2O_3S:Tb$  but lower than those of  $Gd_2O_3S:Tb$ . Therefore, ZnSCdS:Ag could be employed in conventional radiographic applications, for tube voltages up to 80 kVp and for screen coating thicknesses around  $70 \text{ mg cm}^{-2}$ . ZnSCdS:Ag could also be used in digital radiography, since its spectral matching to the Si photodiode is satisfactory. It could also be considered for low-energy applications, since its light output, its electron production efficiency in combination with Si, and its signal to noise ratio (DQE) at low x-ray tube voltages did not significantly differ from those of  $Gd_2O_3S:Tb$ , mostly employed in modern mammography.

### Acknowledgment

This study is dedicated to the memory of Professor G E Giakoumakis, the leading member of our team, whose work on phosphor materials has inspired us.

### Appendix A: Model for absolute luminescence efficiency

The absolute luminescence efficiency is theoretically calculated (Ludwig 1971) by considering that the x-ray absorption, light generation, and light transmission within the screen phosphor material are described by the differential equations

$$dI_f/dt = -(a + s)I_f + sI_b + \frac{1}{2}n_c\mu(E)N_x(E)\exp(-\mu(E)t) \quad (A1)$$

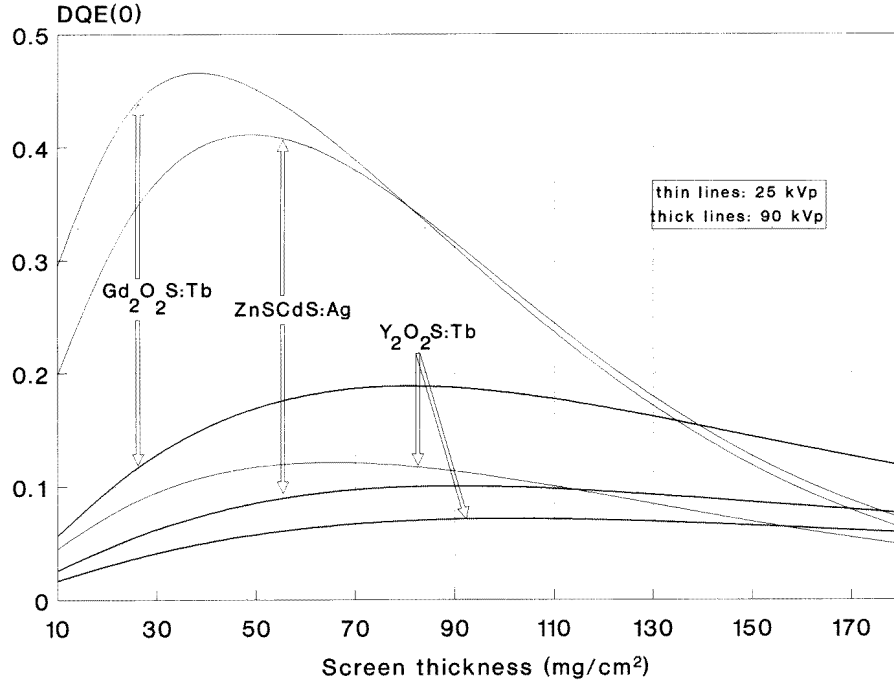


**Figure 12.** Zero-frequency detectable quantum efficiency (DQE(0)) versus screen coating thickness of ZnSCdS:Ag, Gd<sub>2</sub>O<sub>2</sub>S:Tb, and Y<sub>2</sub>O<sub>2</sub>S:Tb phosphors at 90 kVp and 25 kVp.

$$dI_b/dt = (a + s)I_b + sI_f - \frac{1}{2}n_c\mu(E)N_x(E)\exp(-\mu(E)t) \quad (\text{A2})$$

where  $I_f$  and  $I_b$  are the forward and backward directed light intensities relative to x-ray beam directions, corresponding to transmission and reflection modes of measurements respectively.  $N_x(E)$  is the incident x-ray fluence,  $a$  and  $s$  are the light absorption and light scattering coefficients,  $\mu(E)$  is the x-ray mass attenuation coefficient and  $t$  is the penetration depth of x-rays. The solution of these differential equations gives

$$\begin{aligned} \text{AE}(E, T)_{tr} &= \frac{n_c\gamma(E)T_r\mu(E)(1 + \rho)e^{-\mu(E)T}}{2(\mu(E)^2 - \sigma^2)} \\ &\times \frac{(\mu(E) - \sigma)(1 - \beta)e^{-\sigma T} + 2(\sigma + \mu(E)\beta)e^{\mu(E)T} - (\mu(E) + \sigma)(1 + \beta)e^{\sigma T}}{(1 + \beta)(\rho + \beta)e^{\sigma T} - (1 - \beta)(\rho - \beta)e^{-\sigma T}} \end{aligned} \quad (\text{A3})$$

for transmission mode and

$$\begin{aligned} \text{AE}(E, T)_r &= \frac{n_c\gamma(E)\mu(E)e^{-\mu(E)T}}{(\mu(E)^2 - \sigma^2)} \\ &\times \frac{(\mu(E) - \sigma)(\rho + \beta)e^{\sigma T} + 2(\sigma\rho - \mu(E)\beta)e^{-\mu(E)T} - (\mu(E) + \sigma)(\rho - \beta)e^{-\sigma T}}{(1 + \beta)(\rho + \beta)e^{\sigma T} - (1 - \beta)(\rho - \beta)e^{-\sigma T}} \end{aligned} \quad (\text{A4})$$

for reflection mode where  $\text{AE}(E, T)$  is the absolute efficiency in transmission (tr) or reflection (r) modes,  $n_c$  the intrinsic x-ray to light conversion efficiency of the phosphor,

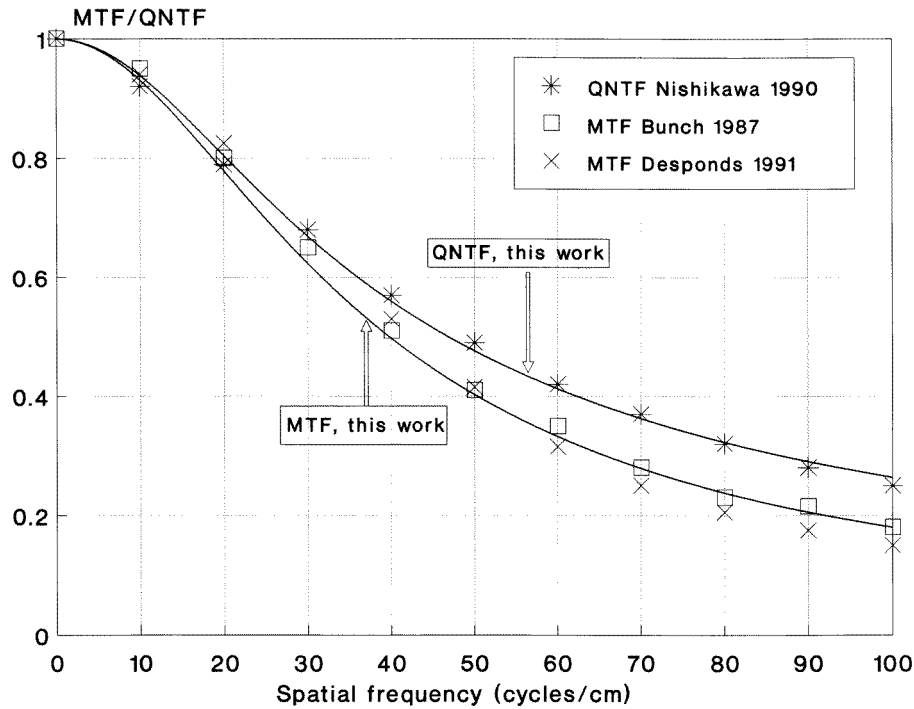


**Figure 13.** A comparison of calculated MTF and QNTF against published experimental MTF (Bunch *et al* 1987, Desponds *et al* 1991) and QNTF (Nishikawa and Yaffe 1988) data for the Kodak Min-R commercial phosphor screen.

$\mu(E)$  the mass attenuation coefficient of the phosphor for the incident x-ray photons,  $T$  the coating thickness of the screen,  $T_r$  the transparency of the screen's substrate,  $\rho = (1 - r)/(1 + r)$  where  $r$  is the reflectivity of the screen's substrate,  $\gamma(E)$  is the conversion factor converting energy fluence ( $\text{W m}^{-2}$ ) into exposure rate ( $\text{mR s}^{-1}$ ), and  $\sigma$  and  $\beta$  are coefficients directly related to the absorption ( $a$ ) and scattering ( $s$ ) coefficients of optical photons within the screen, by

$$\sigma = [a(a + 2s)]^{1/2} \quad \beta = [a/(a + 2s)]^{1/2}.$$

## Appendix B: Models for tungsten and molybdenum x-ray spectra

According to the models of Tucker *et al* (1991a, b) for tungsten and molybdenum x-ray spectra, the number of bremsstrahlung x-ray photons produced with energy between  $E$  and  $E + dE$  is given as

$$N_x(E) dE = [\alpha r_e Z^2 / A] [dE/E] \int_E^{E_0} B \frac{(E_c + m_0 c^2)}{E_e} F(E, E_c, E_0) \left[ \frac{1}{\rho} \frac{dE_e}{dx} \right]^{-1} dE_e \quad (\text{B1})$$

where  $\alpha$  is the fine-structure constant,  $r_e$  is the classical electron radius,  $Z$  is the atomic number of the target,  $A$  is the mass of the target atoms,  $E$  is the x-ray photon energy,  $E_0$  is the kinetic energy of the incident electron,  $E_e$  is the penetrating electron energy,  $m_0$  is the rest mass of an electron,  $c$  is the light velocity,  $(1/\rho)[dE_e/dx]$  is the mass stopping power

of the target material,  $F(E, E_e, E_0)$  is the anode transmitted fraction of x-ray photons given by

$$F(E, E_e, E_0) = \frac{\exp[-\mu(E)(E_0^2 - E_e^2)]}{\rho_a c_{TW} \sin(\vartheta + \varphi)} \quad (\text{B2})$$

where  $\mu(E)$  and  $\rho_a$  are the linear attenuation coefficient and density of the anode material respectively,  $c_{TW}$  is the Thomson–Whiddington constant (Tucker *et al* 1991a, b),  $\theta$  is the target angle,  $\varphi$  is the angle off the central axis along which an x-ray photon travels,  $x$  is the depth of electron penetration within the target and  $B$  is a function of  $Z$  and  $T$  given by Tucker *et al* (1991a, b).

The production of target characteristic x-rays is described by the formula

$$N_x(E_1) = A_K \left[ \frac{E_0}{E_K} - 1 \right]^{n_K} f(E_i) \int_0^R P\left(\frac{x}{R}\right) \exp\left[\frac{-\mu(E_i)x}{\sin(\vartheta + \varphi)}\right] dx \quad (\text{B3})$$

where  $E_K$  is the binding energy of the K shell,  $E_i$  is the energy of the characteristic x-ray photons,  $A_K$  and  $n_K$  are constants,  $f(E_i)$  is the fractional emission of the characteristic x-rays of energy  $E_i$  and  $R$  is the distance at which the average kinetic energy of the electrons becomes equal to  $E_K$ .  $P(x/R)$  is a probability distribution function given by

$$P(x/R) = \frac{3}{2}[1 - (x/R)^2] \text{ for } x \leq R \quad P(x/R) = 0 \text{ for } x > R. \quad (\text{B4})$$

All data for functions and parameters involved in the calculations were taken from the articles by Tucker *et al* (1991a, b).

## References

- Arnold B A 1979 Physical characteristics of screen–film combinations *The Physics of Medical Imaging: Recording System, Measurements and Techniques* ed A G Haus (New York: American Association of Physicists in Medicine) pp 30–71
- Beutel J, Apple B A and Shaw R 1993 The role of screen parameters and print-through in the performance of film/screen systems *Phys. Med. Biol.* **38** 1181–206
- Bunch P C, Huff K E and Van Metter R 1987 Analysis of the detective quantum efficiency of radiographic film–screen combination *J. Opt. Soc. Am. A* **4** 902–9
- Cavouras D, Kandarakis I, Panayiotakis G, Evangelou E K, Nomicos C D 1996 An evaluation of the  $\text{Y}_2\text{O}_3 : \text{Eu}^{3+}$  scintillator for application in medical x-ray detectors and image receptors *Med. Phys.* **23** 1965–75
- Chan H P and Doi K 1983 Energy and angular dependence of x-ray absorption and its effect on radiographic response in screen–film systems *Phys. Med. Biol.* **28** 565–79
- Dainty J C and Shaw R 1974 Detective quantum efficiency, signal to noise ratio, and the noise-equivalent number of quanta *Image Science* (New York: Academic) pp 152–88
- Desponds L, Depeursinge C, Grecescu M, Hessler C, Samiri A and Valley J F 1991 Image quality index (IQI) for screen–film mammography *Phys. Med. Biol.* **36** 19–33
- Dick C E and Motz J W 1981 Image information transfer properties of x-ray fluorescent screens *Med. Phys.* **8** 337–46
- Fahrig R, Rowlands J A and Yaffe M J 1995 X-ray imaging with amorphous selenium: detective quantum efficiency of photoconductive receptors for digital mammography *Med. Phys.* **22** 153–60
- Giakoumakis G E 1991 Matching factors for various light-source–photodetector combinations *Appl. Phys. A* **52** 7–9
- Giakoumakis G E, Nomicos C D, Yiakoumakis E N and Evangelou E K 1990 Absolute efficiency of rare earth oxysulfide screens in reflection mode observation *Phys. Med. Biol.* **35** 1017–23
- Gurwich A M 1995 Luminescent screens for mammography *Radiat. Meas.* **24** 325–30
- Hendee W R 1970 *Medical Radiation Physics* (Chicago: Year Book) pp 145–8
- Kandarakis I, Cavouras D, Panayiotakis G, Agelis T, Nomicos C and Giakoumakis G 1996 X-ray induced luminescence and spatial resolution of  $\text{La}_2\text{O}_2\text{S}:\text{Tb}$  phosphor screens *Phys. Med. Biol.* **41** 297–307
- Karellas A, Harris L J, Liu H, Davis M A, and D’Orsi C J 1992 Charge-coupled device detector: performance considerations and potential for small-field mammographic imaging applications *Med. Phys.* **19** 1015–23

- Ludwig G W 1971 X-ray efficiency of powder phosphors *J. Electrochem. Soc.* **118** 1152–9
- Lumilux Data Book* 1989 (Seelze: Riedel–deHaen)
- Maidment A D and Yaffe M J 1995 Analysis of signal propagation in optically coupled detectors for digital mammography: I. Phosphor screens *Phys. Med. Biol.* **40** 877–89
- Morgan D R, Sones R A and Barnes G T 1987 Performance characteristics of dual-energy detector for digital scan projection radiography *Med. Phys.* **14** 728–35
- Nishikawa, R M and Yaffe M J 1988 *Modeling of the Spatial-frequency-dependent Detective Quantum Efficiency of X-ray Image Receptors*, SPIE vol 914 (Bellingham, WA: SPIE) pp 128–38
- 1990 Model of the spatial-frequency-dependent detective quantum efficiency of phosphor screens *Med. Phys.* **17** 894–904
- Nomicos C D, Giakoumakis G E and Euthymiou P C 1978 Absolute efficiency of (ZnCd)S:Ag phosphor under fluoroscopy conditions *J. Appl. Phys.* **49** 3636–8
- Panayiotakis G, Cavouras D, Kandarakis I and Nomicos C 1996 A study of X-ray luminescence and spectral compatibility of europium-activated yttrium-vanadate (YVO<sub>4</sub>:Eu) screens for medical imaging applications *Appl. Phys.* **62** 483–6
- Press W H, Flannery B P, Teukolsky S A and Vetterling W T 1989 *Numerical Recipes in Pascal: the Art of Scientific Computing* (Cambridge: Cambridge University Press) pp 575–80
- Saloman E B, Hubbell J H and Scofield J H 1988 X-ray attenuation cross-sections for energies 100 eV to 100 keV and elements  $Z = 1$  to  $Z = 92$  *At. Data Nucl. Data Tables* **38** 1–197
- Storm E 1972 Calculated bremsstrahlung spectra from thick tungsten targets *Phys. Rev. A* **5** 2328–38
- Storm E and Israel H 1967 Photon cross-sections from 0.001 to 100 MeV for elements 1 through 100 *Los Alamos Scientific Laboratory of the University of California Report* LA-3753
- Swank R K 1973 Calculation of modulation transfer functions of x-ray fluorescent screens *Appl. Opt.* **12** 1865–70
- 1974 Absorption and noise in x-ray phosphors *J. Appl. Phys.* **44** 4199–203
- Tucker D M, Barnes G T and Chakraborty D B 1991a Semi-empirical model for generating tungsten target x-ray spectra *Med. Phys.* **18** 211–8
- Tucker D M, Barnes G T and Wu X 1991b Molybdenum target x-ray spectra: a semiempirical model *Med. Phys.* **18** 402–7
- Van Metter R and Rabbani M 1990 An application of multivariate moment-generating functions to the analysis of signal and noise propagation in radiographic screen–film systems *Med. Phys.* **17** 65–71
- Zweig G and Zweig D A 1983 Radioluminescent imaging: factors affecting total light output *Proc. SPIE* **419** 297–304